From ill-resolved atomic to ZSM-5 type of ordering in mesoporous lamellar aluminosilica nanoparticles†

Kun Zhang,[a] Yi Meng Wang,*[a] Belén Albela,[b] Li Chen,[a] Ming-Yuan He[a] and Laurent Bonneviot[b]

Received (in Montpellier, France) 13th July 2009, Accepted 24th September 2009
First published as an Advance Article on the web 28th October 2009
DOI: 10.1039/b9nj00331b

Mesoporous lamellar aluminosilicate–surfactant nanoparticles as small as 50 nm can be hydrothermally synthesized at 140 °C using a mixture of cationic and anionic surfactants as a templating agent and tetrapropylammonium cations (TPA^+), known to be the structure directing agent of the MFI type of zeolite. The nanophases exhibit some ill-resolved atomic ordering after 1 to 3 d of crystallization. A definitive ZSM-5 ordering occurs for longer crystallization times, concomitant with a progressive contraction of the lamellar array. In most cases, calcination at 550 °C leads to a collapse of the lamellar structure, while the zeolitic ordering is preserved. For short crystallization times, the lamellar structure with its atomic ordering is maintained when the aluminium source is the nitrate salt, instead of $Al(OH)_3$ or Boehmite. Then, after 3 d of crystallization, highly porous systems are produced with a surface area of $\sim$650 $m^2\ g^{-1}$ and pore volume of $\sim$1.1 $cm^3\ g^{-1}$. For longer crystallization time, the collapse of the lamellar phase under calcination does not affect the well-defined ZSM-5-like atomic ordering and leads to non-faceted nanoparticles of *ca.* 200 nm size with rugged shapes. These conclusion are supported by cross investigations using X-ray diffraction patterns, infrared spectra, scanning electron microscopy and high-resolution transmission electron microscopy with selected area electron diffraction. The ordering of the inorganic sheet of the aluminosilicate–surfactant mesophase is likely favoured by the high diffusion rate of TPA^+ in the nanosized particles.

Introduction

To reduce the diffusion limitation and take full advantage of the catalytic activities of the crystalline microporous zeolite, extensive research efforts have been devoted to synthesizing well-defined mesoporous materials with a molecularly-ordered framework similar to those of conventional zeolite.[1,2] Besides the post-synthesis methods,[3,4] direct synthetic strategies including soft template and hard-template casting techniques are widely used. The former strategy is more intrinsically appealing because of the simplicity of preparation and low cost,[5–11] where dual templates, such as the mesogeneous template of cetyltrimethylammonium (CTA^+) and molecular templates like tetrapropylammonium (TPA^+), are mostly used. However, templates of different nature tend to work in a competitive, rather than a cooperative, manner, leading to an undesirable physical mixture of amorphous MCM-41 and pure zeolite in separate solid phases.[12–14] At best, small cations such as tetramethylammonium (TMA^+) swell the micelles leading to an increased diameter of the mesopores.[15,16] Nonetheless, well characterized single phase hierarchical porous phases have been reported using templates of very different nature such as ammonium molecules and polystyrene beads leading to micro-macroporous interwoven systems.[17] An alternative to direct mixture is the sequential use of templates to generate a small size pore network in an already-made large pore system according to a secondary zeolite crystallization process or to coat the large pore system with nanoparticles of zeolite.[18,19]

However, efforts to impart zeolitic characteristics to lamellar mesoporous silicas and aluminosilicates have met with rather little success. Nonetheless, important milestones should be noted. First, Christiansen *et al.* evidenced what they named the "molecular ordering" of the organic interlayer in a silicate–surfactant layer mesophase with a systematic study of the charge density and the symmetry of the surfactant head group moieties.[20] Later, Wang and Exarhos investigated a study of local "molecular ordering" in layered surfactant–silicate mesophase composites. The temperature, the length of the surfactant chains and the relative amount of TAAOH (tetra-alkylammonium hydroxide, such as TMAOH, TPAOH and TBAOH) to surfactant were found to be critical parameters affecting the local "molecular ordering".[21] These composite mesophases exhibit a local "molecular ordering" within the interlayer organic fillers whereas the inorganic layers remain amorphous in the calcined form. In addition to their instability upon calcination, the absence of aluminium or any other heteroatoms in such silicates does not lead to any interesting

[a] *Shanghai key Lab of Green Chemistry and Chemical Processes, Department of Chemistry, East China Normal University, Shanghai, China. E-mail: ymwang@chem.ecnu.edu.cn; Tel: +86(0)2162232251*
[b] *Laboratoire de chimie, Ecole Normale Supérieure de Lyon, Institut de Chimie de Lyon, Université de Lyon, 46 Allée d'italie, 69364 Lyon cedex 07, France. E-mail: Laurent.bonneviot@ens-lyon.fr*
† Electronic supplementary information (ESI) available: Additional XRD, TEM, SAED and N_2 isotherm data. See DOI: 10.1039/b9nj00331b

chemical reactivity. Recently, Xia and Mokaya reported aluminosilicate materials that exhibit some ordering of the aluminosilicate network that they called "molecular ordering", whereas the "structural ordering" was referring to the lamellar array.[22] A benign template removal treatment using hydrogen peroxide was necessary to keep this fragile structure, proving that this order was effectively associated with the inorganic. Their materials were found to be acidic but exhibited poor textural properties, such as low specific surface area ($<200\ m^2\ g^{-1}$) and pore volume ($<0.30\ cm^3\ g^{-1}$). Unfortunately, these materials are not stable under calcination. Most recently, Ryoo claimed that mesoporous zeolites with tuned mesopore size and higher catalytic activity were synthesized using a rationally designed silane-functionalized surfactant as co-template.[23] However, the sophisticated synthesis of the silane-functionalized surfactant is tedious, costly and of low yield.

Another recent development in the mesoporous community concerned the so-called periodic mesoporous organosilicas (PMO) which may also exhibit molecular scale periodicity.[24–28] This appeared clearly when the organic moieties inserted in the pore wall were aryl groups, which tend to form regular π-stacking. Therefore, the "molecular ordering" of Xia and Mokaya[22] should not be confused with the molecular ordering of organic moieties in PMOs nor template ordering in the lamellar mesophase of Christiansen,[20] since it refers to the inorganic phase only. We decided here to name the local arrangement assigned to the inorganic phase "atomic ordering", the organisation of matter belonging to any organic phase (in the wall or in the interlayer spacing) "molecular ordering" and "structural ordering" is related to supramolecular ordering such as lamellar, hexagonal or cubic mesophases.

It is worth noting that lamellar structures with an amorphous inorganic phase reported up to now are characterized by only few reflection peaks, mostly (100), (200) and (300). In addition to these peaks, molecularly-ordered lamellar phases exhibit X-ray diffraction (XRD) peaks at a higher diffraction angle range associated with the ordered array of the organic spacers. Their poor thermal stability greatly limits their applications since they cannot hold a thermal activation process.

Herein, atomic to zeolitic types of ordering in lamellar mesoporous aluminosilicate have been obtained according to a one-pot synthesis route using a cationic–anionic surfactant mixture of cetyltrimethylammonium bromide (CTABr) and sodium laurate (SL) as a template and TPAOH (tetrapropylammonium hydroxide) as a co-template. The materials prepared using different Al sources were characterized using XRD, scanning electron microscopy (SEM) and transmission electron microscopy (TEM) with selected area electron diffraction (SAED), N_2 adsorption, Fourier transform infrared (FT-IR) spectra and thermogravimetric analysis (TGA). A simple model was proposed to elucidate the formation mechanism of lamellar mesoporous silicas.

Materials and methods

Materials synthesis

In a typical synthesis procedure, 4.67 g of cetyltrimethylammonium bromide (CTABr) and 0.33 g of sodium laurate (SL) was mixed in 102 ml of water and stirred for 1 h at 60 °C until the solution becomes clear. The silicate solution was prepared as follows: 17.5 g of TEOS (tetraethyl orthosilicate) was added drop by drop into a mixture of 34.8 ml of 25% tetrapropylammonium hydroxide (TPAOH) aqueous solution and 22.7 ml of water, and stirred for 30 min. Then, 2.13 g of $Al(NO_3)_3{\cdot}9H_20$ was slowly added into the silicate solution, and this solution was heated to 60 °C and stirred for another 60 min. The silicate solution obtained was slowly added into the mixed template solution. The collected gel composition was SiO_2 : 0.067 Al : 0.153 CTABr : 0.017 SL : 0.50 TPAOH : 100 H_2O. The mixture was stirred continually for 2 h at 60 °C, then loaded into a Teflon-lined steel autoclave, and finally heated under static conditions at 140 °C for a controlled time. Before and after autoclaving, the pH value of the reaction system was recorded. The final products were collected by filtration, washed and dried. To remove the templates, the products were finally heated under air reflux for 6 h at 550 °C. The sample LMS-Al(I)-1d refers to a lamellar silica synthesized using $Al(NO_3)_3{\cdot}9H_20$ as the Al source at 140 °C for 1 day. LMS-Al(II)-*n*d and LMS-Al(III)-*n*d correspond to samples synthesized using aluminium trihydroxide and Boehmite as the Al source, respectively. Note that *n* indicates the number of days of crystallization time. All chemicals were ordered from Sinopharm Chemical Reagent Co.

Characterization

The XRD patterns were collected on a Bruker D8 ADVANCE instrument using Cu Kα radiation (λ = 1.5418 Å) at 40 kV and 40 mA. To get high quality XRD patterns, the scanning times were increased up to 12 h. Nitrogen adsorption–desorption isotherms were recorded at 77 K on a Quantachrome Autosorb-3B instrument after activating the sample under vacuum at 473 K for at least 10 h. The specific surface areas were evaluated using Brunauer–Emmett–Teller (BET) method, and the total pore volume was determined from the amount adsorbed at a relative pressure of about 0.99. The pore size distribution curves were calculated from the analysis of the desoprtion branch of the isotherms using Barret–Jovner–Halenda (BJH) algorithm. The SEM images were taken on a Hitachi S-4800 microscope. Transmission electron microscopy (TEM) experiments were conducted on a JEOL 2011 microscope (Japan) operated at 200 kV. FT-IR spectra were recorded on a Nicolet Fourier transform infrared spectrometer (NEXUS 670) using the KBr technique. Thermogravimetric analysis (TG) was performed using a Perkin-Elmer TGA analyzer with a heating rate of 10 °C min^{-1} under an air flow.

Results and discussion

XRD patterns

Powder XRD patterns for the as-synthesized and calcined materials are shown in Fig. 1. The low-angle XRD patterns ($2\theta < 7°$) of all as-synthesized samples in Fig. 1A exhibit a strong peak at *ca.* 3°, a much weaker one at *ca.* 6° and a very weak peak at *ca.* 9°. The peaks are rather large and can be attributed to the (100), (200) and (300) directions of a lamellar

phase with a short ordering range (~50 nm). When the crystallization time was extended from 1 to 7 d, the d_{100} value shifts from 3.77 to 2.88 nm, and the peaks gradually broaden, implying a shorter range of ordering. Most interestingly, the XRD patterns of as-synthesized mesophases also exhibit some broad or sharp diffraction peaks in the wide-angle region (2θ between 10 and 35°). For 1 d crystallization time, a slightly asymmetric broad band arises between 16 to 27°. This is mainly due to the scattering of the randomly-oriented Si–Si and Si–Al pairs, the separation distance of which spans from 2.9 to 3.3 Å; this characterizes the amorphous pore wall.[29] When the crystallization time was extended to 3 d, the shape of the broad peak changes with a flat top from 20 to 24.0° and a sharper feature at 25°. This indicate a strong change from a pure statistical distance distribution to some non-statistical one. This is the fingerprint of some atomic ordering of the aluminosilicate network, reported earlier as a "molecularly ordered" inorganic phase.[20–22] After longer crystallization times of 5 to 7 d, several new sharp peaks, centered at 2θ = 7.9, 8.9 and 23°, are observed, fully consistent with the MFI structure of ZSM-5.[30]

The XRD patterns of calcined samples are depicted in Fig. 1B. After crystallization for 1 d, the low angle diffraction peaks, assigned to the ill-resolved lamellar phase on the as-made materials, are still present after calcination. This implies that the collapse of the mesophase is hindered by the connection of the layer with other intergrown hexagonal or cubic mesophases. The reasoning invoked previously for thermally stable lamellar phases templated with surfactant having crown ether polar head groups may apply here.[31] Another possibility could be the pillaring effect of some inorganic oligomeric species that may intercalate in-between the layers in the ill-formed phase. In aluminium nitrate solution, in the basic conditions used here, Keggin-like Al_{13} species of about 1 nm diameter are known to form.[32] For crystallization times of 3 d or more, the disappearance of the low diffraction angle peaks shows that calcination leads to the collapse of the lamellar phase. Meanwhile, the wide-angle XRD pattern showed no peak centered at 25°, indicating that the atomic order is destroyed as observed by Mokaya *et al.*[22] For prolonged crystallization time up to 5 or 7 d, the characteristic XRD peaks of MFI structure remained after calcination. When aluminium trihydroxide and Boehmite were used as the aluminium source, the as-made LMS-Al(II) and LMS-Al(III) materials showed very similar XRD patterns at low angles and almost no ZSM-5 (very small peaks at wide angles (Fig. S1, ESI†). There is retention of the lamellar phase in these cases.

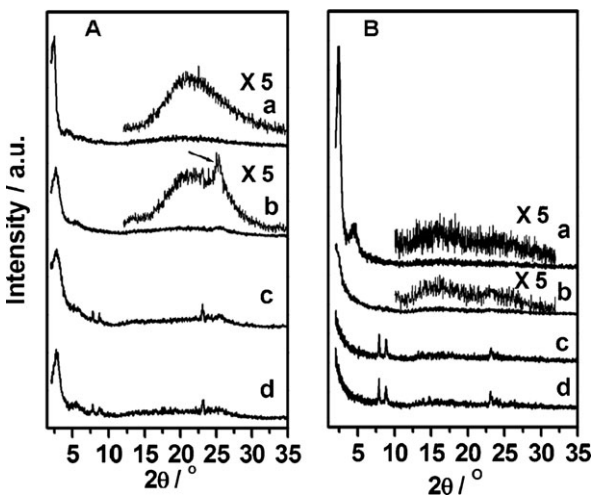

Fig. 1 Powder XRD patterns of molecularly-ordered lamellar silicate–surfactant mesophases, LMS-Al(I) : before (A) and after (B) calcination in a 2θ range 2–35°. LMS-Al(I): for (a) 1, (b) 3, (c) 5 and (d) 7 d.

SEM characterization

The grain morphology obtained from SEM is often characteristic of the grain crystallinity and symmetry and may provide information on the growth mecanism.[33,34] Typical SEM images of the as-synthesized samples are shown in Fig. 2 at different crystallization times (Fig. 2). In the case of $Al(NO_3)_3$ as Al source, nanoparticles with narrow size distribution (~50 nm) are observed at the shorter crystallization time of 1 d (Fig. 2(a)). After 3 d crystallization time (Fig. 2(b)), the particles exhibit unique spherical aggregates 200 nm in size and no faceted crystal of MFI structure is observed. When the crystallization time is further extend to 5 and 7 d (Fig. 2(c) and (d)), the size and the shape of particles are not changed. It is worth noting here that only a few articles have reported the synthesis of mesostructured particles with sizes less than 100 nm.[34,35]

By contrast, the morphologies of LMS-Al(II) and LMS-Al(III) exhibit much larger non-faceted rough particles from 5 to 40 μm, after 1 d of crystalization, that are consistent with a layered structure (Fig. 3a and d). After 3 d of crystallization, the particles become spherical and slightly smaller, ranging from 5 to 12 μm (Fig. 3b and e). Their surface is rough, looking like "sand roses". Some MFI coffin-shaped microcrystals of about 5 μm are also observed. A close observation of these latter particles reveals a roughness due to small interwoven plates (Fig. 3c and f). This suggests that undissolved layered aluminium trihydroxide or Boehmite phases may act as a nanobinder or a nucleus favouring plate-like nanocrystals assembling into larger rugged surface particles. There is

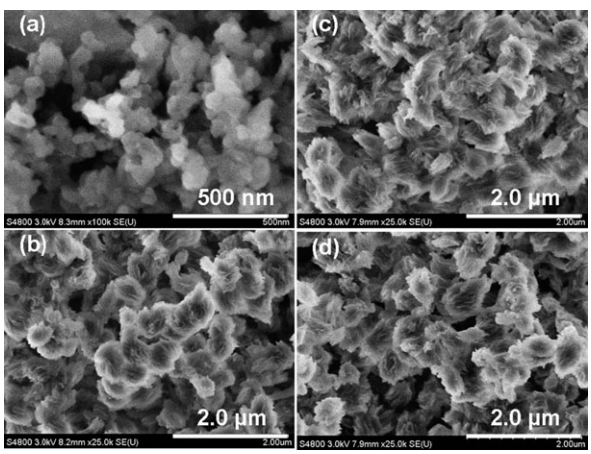

Fig. 2 SEM images of as-synthesized LMS-Al(I) for (a) 1, (b) 3, (c) 5 and (d) 7 days.

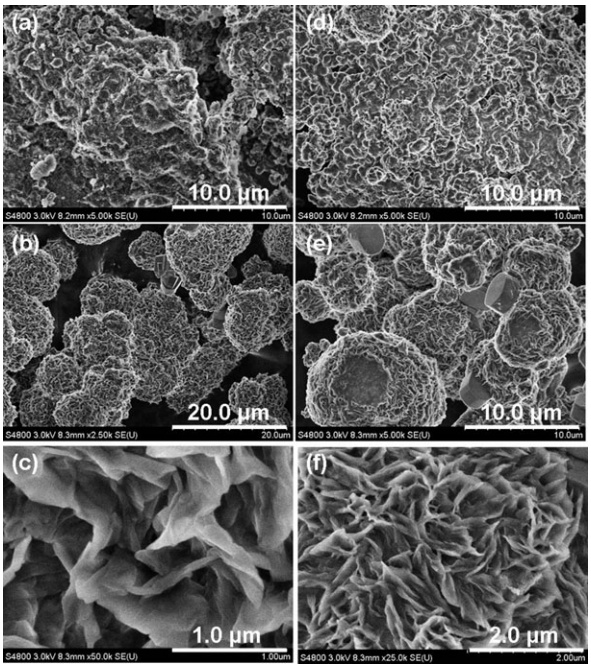

Fig. 3 SEM images of the as-synthesized lamellar mesophase. Samples (a), (b) and (c) were synthesized at 140 °C, using $Al(OH)_3$ as the Al source for 1 and 3 d, respectively. Samples (d), (e) and (f) were synthesized at 140 °C, using Boehmite as the Al source, for 1 and 3 d. Note that (c) and (f) are high-magnification SEM images of (b) and (e).

definitively a strong effect of the aluminium precursor on the crystal growth of the lamellar phase.

It is well known that nanosized porous materials have a large external surface area and short diffusion path, which significantly improves the mass-transfer rate in the confined space, and thus exhibit high chemical reactivity.[36] So intercalation of species is more likely to occur in the nanoparticles of LMS-Al(I) (50–200 nm) than in those of LMS-Al(II) or LMS-Al(III) materials (5–10 μm). Indeed, small tetraalkylammonim cations, such as TMA^+ (tetramethylammonium) and TEA^+ (tetraethylammonium), can easily exchange with the template in the channel of 2D hexagonal MCM-41 silica,[37] or enter in the templating micelles in the mesophase as reported by Corma's and Sayari's groups.[15,16] Here, in the hydrothermal condition, TPA^+ molecules may diffuse into the channels or the interlayer spacing and move progressively into the amorphous pore walls to generate crystalline-like inorganic frameworks. When aluminium trihydroxide and Boehmite are used, the much larger particles may explain the poor diffusion of TPA and the low yield of formation of ZSM-5. Furthemore, the collapse of the lamellar array is not consistent with the hypothesis of intergrown lamellar and hexagonal or cubic mesophases.

HR-TEM observation

The high-resolution TEM brings complementary information at a lower scale of length than SEM and was applied here as in previous reports on the topic.[27–29,33,34] Fig. 4 shows the TEM images and SAED patterns (inset figure) of samples with $Al(NO_3)_3$ as the Al source. After 1 d crysallization time, the

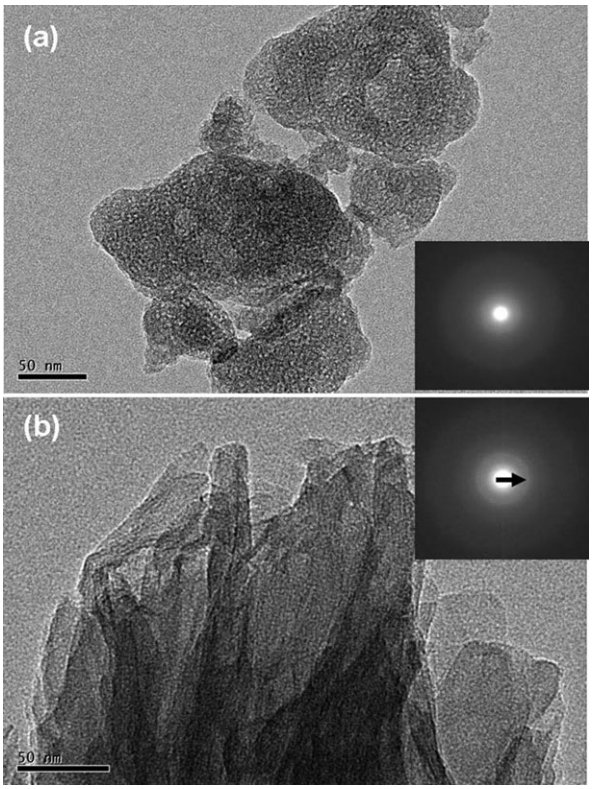

Fig. 4 TEM and SAED (inset) of LMS-Al(I): (a) and (b) synthesized at 140 °C for 1 and 5 d, with $Al(NO_3)_3$ used as the Al source (arrow in the insert indicates the presence of a diffuse diffraction ring).

materials exhibit an internal structure that is most likely worm-like, in-between lamellar in some cases and hexagonal in some other cases. The particles of irregular shape fall in a range of less than 100 nm, consistent with the SEM observations. For crystallization of 5 d or more, the phase is purely lamellar. After 3 d of crystallization, the TEM picture is a mixture of worm like and pure pillared lamellar structure (Fig. S3, ESI†). These TEM observations are consistent with the XRD results.

Selected area electron diffraction (SAED) (Fig. 4, inset) doesn't show any crystalline character (*i.e.* the absence of a diffuse diffraction ring), similar to the amorphous MCM-41 silica. However, if crystallization time was prolonged to 5 d, the SAED shows the presence of a diffuse diffraction ring that is an indication that these particles exhibit some atomic ordering. This may be related to secondary building units of microporous zeolites generated by TPA.[20,29] So far, these secondary building units (SBUs) have not been directly observed by any regular measurements, for instance HR-TEM, nor from solid state NMR. The most direct proof of the existence of SBUs was obtained by a mass spectrometry investigation of the synthesis mother solution from Schüth *et al.*[40] To further evidence the presence of the SBU in our samples, the FT-IR spectroscopy was carried out.[41–43]

IR spectrum

The FT-IR spectra of LMS-Al(I) are shown in Fig. 5. The 1000–1100 and 800 cm^{-1} absorptions attributed to Si–O asymmetric and symmetric stretching vibrations, along with

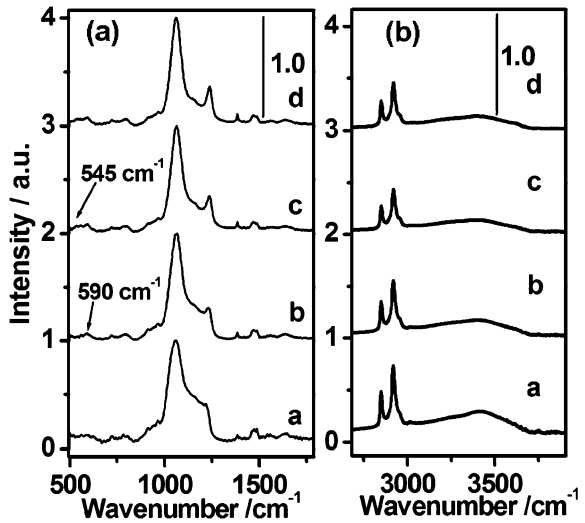

Fig. 5 IR spectra of as-synthesized lamellar aluminosilicate–surfactant mesophases, LMS-Al(I): for (a) 1, (b) 3, (c) 5 and (d) 7 d.

719 and 730 cm^{-1} absorptions arising from the surfactant species are not specific to atomic ordering in the zeolite phase. By contrast, the 500–650 cm^{-1} region provides information on specific silicate rings typical of the zeolitic structure. Indeed, both LMS-Al(I)-1d and LMS-Al(I)-3d samples show a single adsorption band centered at 590 cm^{-1}. A similar result was also reported by Christiansen *et al.* for the so-called "molecularly ordered" silicate lamellar materials.[20] However, a precise assignment of this band remains to be done. When crystallization time is extended to 5 d, another band, centered at 545 cm^{-1}, appears indicating the presence of five-membered rings typical of the pentasil zeolite family to which MFI zeolites belong. This is consistent with the XRD results and further confirms the progressive atomic ordering of the mesoporous lamellar aliminosilicates.

The evolution of organic species in the material is quantatively monitored from the IR adsorption bands intensities normalized using the band at ~1060 cm^{-1} as a reference.[37] In Fig. 5(b), the absorption bands at 2958 and 2870 cm^{-1} are assigned to the symmetric and asymmetric CH_2 stretching modes in long C-16 hydrocarbon chains of CTA^+, respectively. With increasing crystallization time, the intensity of these two bands decreases by 20, 40 and 40 % after 3, 5 and 7 d respectively, indicating that CTA^+ molecules are partially removed out of the channels. Interestingly, a new sharp absorption at 1380 cm^{-1}, characteristic of nitrate anions, was observed, the intensity of which reached a maximum value for 5 d crystallization time. The incorporation of nitrate anions may indicate that Keggin-like species are possibly introduced into the channels because the ion-exchange process of such multicharged Al_{13} species must be accompanied by counter anions.

TG analysis

In Fig. 6, the weight loss between 100 and 400 °C is likely due to the decomposition of CTA^+. TGA shows that the molar ratio of CTA^+/silica decreases from 0.152 to 0.110 when crystallization time is extended from 1 to 5 d. This ratio increases again up to 0.135 for a crystalline time of 7 d. In addition, the derivative TG curves (DTG) of all the samples in Fig. 6(b) shows a small peak centered at 400 °C, corresponding to the thermal decomposition of TPA^+ molecules. This indicates that TPA^+ molecules can enter into the channel.[44] This probably occurs *via* partial ion exchange of CTA^+ molecules by TPA^+ molecules, a reaction which is already known.[15,16,37] These observations also suggest that the atomic ordering of inorganic frameworks of current lamellar phases are directed by TPA^+ molecules.

Nitrogen physisorption isothems

Up to now, the reported calcined lamellar mesophase exhibits low textural properties. On the contrary, the actual atomically-ordered aluminosilicate–surfactant mesophases retain high porosity characteristics, summarized in Table 1. The adsorption–desorption isotherm for sample LSM-Al(I)-1d is a typical type IV isotherm with a sharp inflection point at relative pressure 0.2–0.35 due to capillary condensation, as shown in Fig. 7(a). This inflection is characteristic of mesoporous materials. Most interestingly, the isotherm of the LSM-Al(I)-3d sample shows an increase in the total pore volume from 0.98 to 1.08 $cm^3\ g^{-1}$ and a slight decrease in the surface area from 843 to 655 $m^2\ g^{-1}$. In addition, the inflection point decreases in sharpness and shifts to lower relative pressure value, corresponding to a decrease of the mesopore size from 2.5 to 2.2 nm, calculated by the BJH method in Fig. 7(b). This is consistent with the contraction observed from XRD. Prolonging the crystallization time leads to a drastic decrease of the BET surface area and the BJH pore size analysis does not show any mesopores in the calcined samples. This implies that the as-made pillar lamellar mesophases are completely transformed into pure lamellar mesophases, as suggested by XRD analysis. It is worth noting that, after calcination, this pure lamellar mesophase shows a much higher pore volume than that of the corresponding lamellar phase synthesized using aluminium trihydroxide and Boehmite as Al sources (Fig. S4, ESI†).

The presence of hysteresis between the adsorption and desorption isotherms could be observed due to the capillary condensation, particularly at relative pressures greater than 0.4. At P/P_0 above 0.8, all the isotherms of LSM-Al(I) samples

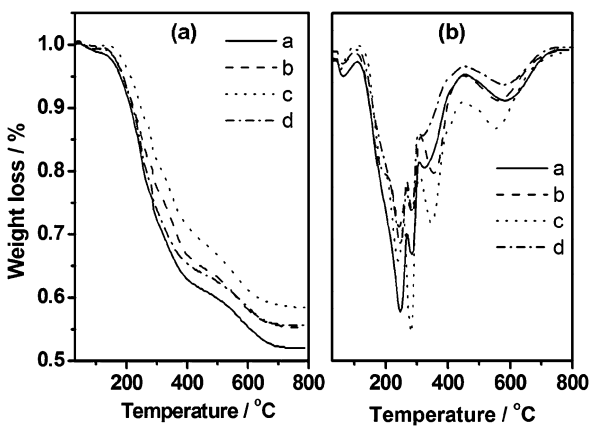

Fig. 6 TGA (a) and derivative TGA (b) of LMS-Al(I) for (a) 1, (b) 3, (c) 5 and (d) 7 d.

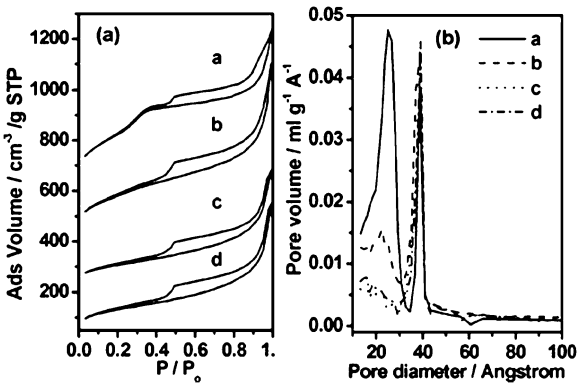

Fig. 7 Nitrogen physisorption isothems (left) and pore size distribution plot calculated by BJH method from desorption branch (right) of calcined lamellar mesophases. LMS-Al(I): for (a) 1, (b) 3, (c) 5 and (d) 7 d.

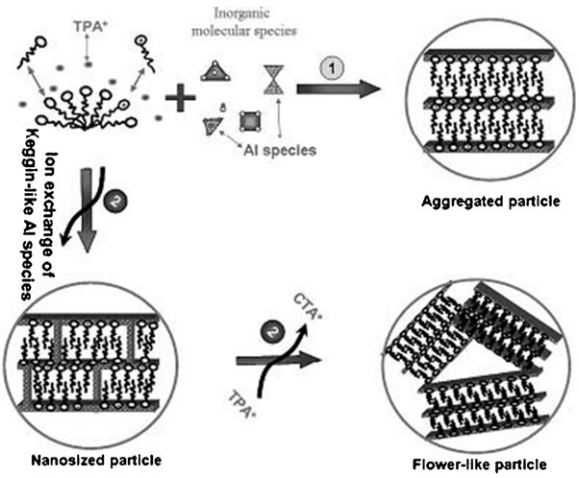

Scheme 1 Proposed mechanism for the formation of lamellar silicate–surfactant mesophases.

are characterized by very steep adsorption into large mesopores with pore size larger than 7.0 nm, which is associated with the packing voids between nanoparticles. A similar hysteresis loop at higher relative pressure was reported by Mokaya and his coworkers, and they explained that this type of porosity arises also from interparticle voids.[22] This latter type of porosity might drastically accelerate the diffusion of large molecules into the channels, such as TPA^+ molecules, consequently favouring the formation of lamellar silicate–surfactant mesophases with a crystalline inorganic framework. However, the samples synthesized using Boehmite and aluminium trihydroxide as the Al source show no significant adsorption at relative pressure larger than 0.8 (Fig. S4, ESI†).

Formation mechanism

A simple model is proposed to elucidate the formation mechanism of the actual atomically ordered lamellar aluminosilicate–surfactant mesophases as depicted in Scheme 1. In general, the lamellar mesostructure will disappear after surfactant removal during the calcination, if there is no pillaring in the interlayer spacing as described in route 1. When Boehmite is used as the Al source, the calcined samples show poor textural properties due to the destruction of the lamellar mesostructure. When $Al(NO_3)_3$ is used in synthetic route 2, nanosized particles with narrow size distribution centered at 50 nm were synthesized at short crystallization times. The corresponding LSM-Al(I)-1d sample keeps fairly well defined lamellar mesostructure and exhibits a large pore volume and a high surface area after the calcination. This suggests that this nanosized particle is composed of pillared lamellar silicate–surfactant mesophases as described in route 2.

Since hydrolysis and polymerization of $Al(NO_3)_3$ under basic conditions may lead to the formation of Keggin-like or other polymeric Al species,[32] the adsorption of such Al_{13} oligomeric species on the surface of lamellar mesophase nuclei may hinder the growth of final particles, explaining the nanosized particles observed. Meanwhile, these oligomers may act as a pillaring agent. The role of the oligomeric species during the hydrothermal synthesis needs more investigation to be confirmed. Longer crystallization times yield non-pillared lamellar aluminosilicate–surfactant mesophases since the oligomeric species get progressively dissolved.

In addition, due to the ion exchange reaction between CTA^+ and TPA^+ molecules, the latter may migrate into the channels and concomitantly conduct the amorphous pore wall to a progressively atomic ordering of the inorganic framework. Note that the high molar ratio of TPA^+/CTA^+ ($\sim$3.3) in the initial precursor gel promotes more TPA^+ molecules to migrate into the channels, similar to the results reported by Corma and Sayari.[15,16] Finally, homogeneous atomic ordering all through the aluminosilicate–surfactant mesophases is produced by TPA^+, with very little morphology change during the hydrothermal transformation from amorphous wall to crystalline-like inorganic framework.[45–47] This looks like the pseudomorphous transformation of monoliths of silica

Table 1 Textural property of calcined lamellar silicate–surfactant materials

Name	d_{100}[a]/nm	S_{BET}[b]/m^2 g^{-1}	V_t[c]/cm^3 g^{-1}	D_{BJH}[d]/nm	S_{mi}[e]/m^2 g^{-1}	V_{mi}[f]/cm^3 g^{-1}	S_{meso}/m^2 g^{-1}	V_{meso}/cm^3 g^{-1}
LMS-Al(I)-1d	3.74	843	0.98	2.5	0	0	843	0.98
LMS-Al(I)-3d	3.27	655	1.08	2.2	0	0	655	1.08
LMS-Al(I)-5d	3.15	367	0.75	—	32	0.02	335	0.73
LMS-Al(I)-7d	2.88	442	0.85	—	76	0.04	365	0.81
LMS-Al(II)-1d	3.58	648	0.78	—	0	0	0	0.78
LMS-Al(II)-3d	2.81	397	0.43	—	92	0.05	305	0.36
LMS-Al(III)-1d	3.01	260	0.23	—	84	0.05	176	0.18

[a] d_{100} measured from XRD patterns. [b] BET surface area measured in the P/P_0 range 0.1–0.25 with uncertainty = $\pm$30 m^2 g^{-1}. [c] Total pore volume measured at P/P_0 = 0.99, uncertainty = $\pm$0.02 cm^3 g^{-1}. [d] Mesopore size using BJH calculation from desorption branch. [e] Micropore surface area using *t*-plot calculation. [f] Micropore volume using *t*-plot calculation.

into mesoporous monoliths reported by Galarneau *et al.*, or the secondary zeolite crystallization process in SBA-15 large pore wall by On *et al.*[3,48]

Conclusions

Ill-resolved atomic and ZSM-5 types of ordering in lamellar aluminosilicate–surfactant mesophases with a Si/Al molar ratio of 15 are obtained using a cationic and anionic surfactant mixture as a template and tetrapropylammonium (TPA^+) as a structure directing agent (SDA). The success of the current synthetic route relies on the nanosized lamellar phase that allows a short diffusion path and greatly accelerates the diffusion rate of large molecules in the confined interlayer space, such as TPA^+ molecules. Then, the inserted TPA^+ molecules can conduct the transformation of the armorphous pore wall from mere local atomic ordering towards crystalline-like frameworks. Particle size control is therefore a key issue that depends on the choice of Al source. Local atomic ordering is proved by X-ray diffraction patterns, Fourier transformed infrared spectra and high-resolution transmission electron microcopy. In addition, SEM identifies that the lamellar mesophases with a crystalline-like framework are homogeneously distributed without any separate MFI structured zeolite phase. Nitrogen physisorption isotherms show that these novel lamellar mesophases exhibit high porous characteristics after calcination. The challenge remains here to find a better compromise between the lamellar collapse and high atomic ordering to complete the zeolitic structure within the inorganic layers. Efforts are underway to take advantages of this better understanding of the internal crystallization within a nano-structure framework to design mesoporous zeolites with true hierarchical porosity.

Acknowledgements

This work is supported by the National Science Foundation of China (key project 20890122) and Shanghai Leading Academic Discipline Project (Project B409). Ms Xia-Li Zhang and Prof. Dong-Yuan Zhao from Fudan University are also warmly acknowledged for HR-TEM measurements.

Notes and references

1 A. Corma, *Chem. Rev.*, 1997, **97**, 2373.
2 Y. Wan and D. Y. Zhao, *Chem. Rev.*, 2007, **107**, 2821–2860.
3 D. T. On and S. Kaliaguine, *Angew. Chem., Int. Ed.*, 2001, **40**, 3248.
4 D. T. On and S. Kaliaguine, *J. Am. Chem. Soc.*, 2003, **125**, 618.
5 K. R. Kloetstra, H. Van bekkum and J. C. Jansen, *Chem. Commun.*, 1997, 2281.
6 Z. Zhang, Y. Han, L. Zhu, R. Wang, Y. Yu, S. Qiu, D. Zhao and F.-S. Xiao, *Angew. Chem., Int. Ed.*, 2001, **40**, 1258.
7 Z. Zhang, Y. Han, F.-S. Xiao, S. Qiu, L. Zhu, R. Wang, Y. Yu, B. Zou, Y. Wang, H. Sun, D. Zhao and Y. Wei, *J. Am. Chem. Soc.*, 2001, **123**, 5014.
8 Y. Liu, W. Z. Zhang and T. J. Pinnavaia, *J. Am. Chem. Soc.*, 2000, **122**, 8791.
9 Y. Liu, W. Z. Zhang and T. J. Pinnavaia, *Angew. Chem., Int. Ed.*, 2001, **40**, 1255.
10 L. Huang, W. Guo, P. Deng, Z. Xue and Q. J. Li, *J. Phys. Chem. B*, 2000, **104**, 2817.
11 W. P. Guo, C. R. Xiong, L. M. Huang and Q. J. Li, *J. Mater. Chem.*, 2001, **11**, 1886.
12 P. H. R. P. Poladi and C. C. Landry, *J. Solid State Chem.*, 2002, **167**, 363.
13 P. H. R. P. Poladi and C. C. Landry, *Microporous Mesoporous Mater.*, 2002, **52**, 11.
14 S. M. Solberg, D. Kumar and C. C. Landary, *J. Phys. Chem. B*, 2005, **109**, 24331.
15 A. Corma, Q. Kan, M. T. Navarro, J. Perez-Pariente and F. Rey, *Chem. Mater.*, 1997, **9**, 2123.
16 M. Kruk, M. Jaroniec and A. Sayari, *J. Phys. Chem. B*, 1999, **103**, 4590.
17 S. Vaudreuil, B. Echchahed, P. Reinert, M. Bousmina, S. Kaliaguine and L. Bonneviot, *J. Porous Mater.*, 2007, **14**, 173.
18 R. A. Farrell, N. Petkov, H. Amenitsch, J. D. Holmes and M. A. Morris, *J. Mater. Chem.*, 2008, **18**, 2213.
19 X.-J. Meng, F. Nawaz and F. S. Xiao, *Nano Today*, 2009, **4**, 292.
20 S. C. Christiansen, D. Zhao, M. T. Janicke, C. C. Landry, G. D. Stucky and B. F. Chmelka, *J. Am. Chem. Soc.*, 2001, **123**, 4519.
21 L. Q. Wang and G. J. Exarhos, *J. Phys. Chem. B*, 2003, **107**, 443.
22 Y. Xia and R. Mokaya, *J. Phys. Chem. B*, 2006, **110**, 9122.
23 M. Choi, H. S. Cho, R. Srivastava, C. Venkatesan, D. H. Choi and R. Ryoo, *Nat. Mater.*, 2006, **5**, 718.
24 M. P. Kapoor and S. Inagaki, *Bull. Chem. Soc. Jpn.*, 2006, **79**, 1463.
25 S. Fujita and S. Inagaki, *Chem. Mater.*, 2008, **20**, 891.
26 B. Hatton, K. Landskron, W. Whitnall, D. Pervoic and G. A. Ozin, *Acc. Chem. Res.*, 2005, **38**, 305.
27 A. Sayari and W. Wang, *J. Am. Chem. Soc.*, 2005, **127**, 12194.
28 Y. Yang and A. Sayari, *Chem. Mater.*, 2007, **19**, 4117.
29 R. Mokaya, *Chem. Commun.*, 2001, 1092.
30 H. Van Koningsveld, H. Van Bekkum and J. C. Jansen, *Acta Cryst. B*, 1987, **43**, 127.
31 C. Danumah, S. M. J. Zaidi, G. Xu, Normand Voyer, S. Giasson and S. Kaliaguine, *Microporous Mesoporous Mater.*, 2000, **37**, 21.
32 V. Francetiĉ and P. Bokovec, *Acta Chim. Slov.*, 2008, **55**, 904.
33 D. P. Serrano, M. A. Uguina, G. Ovejero, R. Van Grieken and M. Camacho, *Microporous Mater.*, 1996, **7**, 309.
34 S. Sadasivan, C. E. Fowler, D. Khushalani and S. Mann, *Angew. Chem., Int. Ed.*, 2002, **41**, 2151.
35 K. Möller, J. Kobler and T. Bein, *Adv. Funct. Mater.*, 2007, **17**, 605.
36 J. Pérez-Ramírez, C. H. Christensen, K. Egeblad, C. H. Christensen and J. C. Groen, *Chem. Soc. Rev.*, 2008, **37**, 2530.
37 K. Zhang, B. Albela, M. Y. He, Y. M. Wang and L. Bonneviot, *Phys. Chem. Chem. Phys.*, 2009, **11**, 2912.
38 D. D. Liang, L. Follens, A. Aerts, J. A. Martens, G. Van. Tendeloo and C. A. Kirschhock, *J. Phys. Chem. C*, 2007, **111**, 14283.
39 S. Lee, Y. Han, M. Park, G. Park and J. Choy, *Chem. Mater.*, 2003, **15**, 4841.
40 S. A. Pelster, W. Schrader and F. Schüth, *J. Am. Chem. Soc.*, 2006, **128**, 4310.
41 P. A. Jacobs, H. K. Beyer and J. Valyon, *Zeolites*, 1981, **1**, 161.
42 J. C. Jansen, F. G. van der Gaag and H. van Bekkum, *Zeolites*, 1984, **4**, 369.
43 A. Tuel, *Chem. Mater.*, 1999, **11**, 1865.
44 S. Mintova, M. Hölzl, V. Valtchev, B. Mihailova, Y. Bouizi and T. Bein, *Chem. Mater.*, 2004, **16**, 5452.
45 D. P. Serrano and R. Van Grieken, *J. Mater. Chem.*, 2001, **11**, 2391.
46 J. H. Choy, S. R. Lee, Y. S. Han, M. Park and G. S. Park, *Chem. Commun.*, 2003, 1992.
47 M. Choi, K. Na and R. Ryoo, *Chem. Commun.*, 2009, 2845.
48 B. Lefèvre, A. Galarneau, J. Iapichella, C. Petitto, F. Di Renzo, F. Fajula, Z. Bayram-Hahn, R. Skudas and K. Unger, *Chem. Mater.*, 2005, **17**, 601.